2011 11th IEEE-RAS International Conference on Humanoid Robots
Bled, Slovenia, October 26-28, 2011

Optimization and Control of Cyclic Biped Locomotion on a Rolling Ball

Yu Zheng, Katsu Yamane

Abstract— **This paper investigates the optimization and control of biped walking motion on a rolling cylinder. We design a balance controller for a simplified linear model of a biped robot, which comprises a foot connected to a lump mass through an ankle joint and a translational spring and damper. We also derive a collision model for the system consisting of the cylinder, supporting leg, and swing leg. With the balance controller and collision model, the robot motion is uniquely determined by the initial state. We can therefore optimize the initial state so that the robot achieves a cyclic gait with a constraint on the desired average rolling velocity. Once an optimal initial state is obtained, we further discuss how to maintain the cyclic motion under disturbances. More specifically, we present a method for computing the joint angles and velocities of the swing leg before it collides with the cylinder. The optimization and control results are demonstrated in simulation.**

I. Introduction

Building a robot, which not only looks but also behaves like a human or even becomes more capable than a human, is one of the ultimate goals in humanoid robotics. Researchers have developed robots that are capable of normal human activities such as walking [1] and running [2] as well as tasks that are difficult for humans such as flipping [3] and juggling [4]. Most of these robots assume static and controlled environment or specialized hardware.

In order to deal with disturbances and uncertainties in the real environment, researchers have also developed techniques of control and planning under dynamic environments [5], [6], [7] and external disturbances [8], [9], [10]. However, these techniques are focused on passive adaptation to dynamic changes in the environment. Although researchers started to take advantage of dynamic environments in the context of object manipulation [11], very few work has been done in whole-body motion control of biped humanoid robots.

The goal of this research is to realize a generic biped humanoid robot that actively manipulates the environment to perform dynamic motions. In this particular piece of work, we choose walking on a cylinder as an example of such behaviors. Walking on a cylinder is difficult even for normal humans. Considering the cylinder movement is mandatory because the interaction with the environment is limited to the contact between the cylinder and floor.

We have studied this problem using a simplified model of the system shown in Fig. 1(a), where the robot dynamics is represented by a wheeled inverted pendulum that is controlled by a state-feedback balance controller. The motion of the simplified model is mapped to a biped model by a footstep planner [12]. However, the footstep planner maps the motion in a geometric way and does not consider the collision between the swing foot and the cylinder. In addition, this model corresponds to the case where the feet can maintain surface contact with the cylinder, which is difficult unless the robot's feet are flexible as human feet.

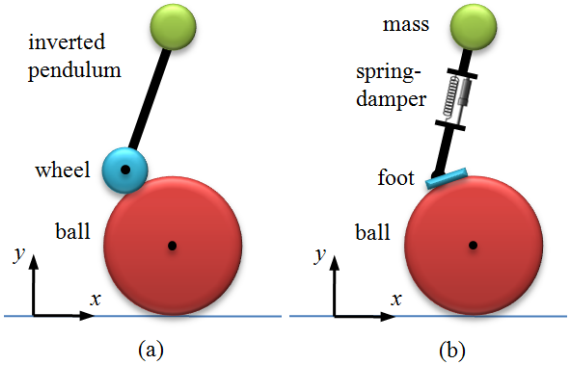

Fig. 1. Different simplified dynamics models of a biped robot on a cylinder in the sagittal plane. (a) An inverted pendulum with a wheel used in [12]. (b) An inverted pendulum with a foot used in this paper.

In this paper, in contrast, we present a generic cyclic gait planner that takes the collision into account together with other constraints such as the friction constraint and constraint on the center of pressure (CoP). We also use a new simplified dynamics model that corresponds to point contact feet, as shown in Fig. 1(b), and design a state-feedback balance controller using pole assignment or linear quadratic regulator as described in [12] after linearizing the model. The model comprises a foot segment connected to a lump mass via the ankle joint and translational spring and damper. The major difference from the model used in [12] is that only one equilibrium state can be used as the reference state for the new model, i.e., standing upright on top of the cylinder. Owing to this, generating a sequence of steps for the new model would be more difficult. This also motivates us to develop such a cyclic gait planner. The proposed cyclic gait planner can also be used for the model in [12].

We develop two new methods for the new model. We first describe a method for determining an initial state of the supporting leg that realizes a cyclic gait for given step duration and average velocity. Because there is only one equilibrium state that can be used as the reference state of the balance controller, the motion of the supporting leg is uniquely determined by its initial state. The method also requires a collision model that describes the relationship

Yu Zheng is with the Department of Computer Science, University of North Carolina at Chapel Hill, NC 27599, USA. This work was done when he was with Disney Research Pittsburgh, PA 15213, USA. yuzheng001@gmail.com

Katsu Yamane is with Disney Research Pittsburgh, PA 15213, USA. kyamane@disneyresearch.com

between the velocities of the swing leg before and after a collision. We also analyze the properties of obtained cyclic gaits, such as energy consumption and robustness.

The state of the supporting leg at the end of a cycle may differ from a planned gait due to modeling errors and external disturbances. We therefore develop a method for determining the state of the swing leg before collision so that the robot can maintain the planned cyclic gait. The method solves a collision equation similar to the one used in the first method.

This paper is organized as follows. Section II summarizes the related work. Section III introduces the balance controller and collision model. Sections IV and V discuss our methods. Simulation results are given in Section VI, followed by conclusions in Section VII.

II. Related Work

A common approach to humanoid locomotion planning is to generate a pattern in which the zero-moment point (ZMP) stays in the contact convex hull. For control, this approach usually assumes that the feet make flat contact with the ground so that the ZMP can deviate from the planned position to deal with disturbances. Unfortunately, we cannot directly apply this approach to our problem because we would have to modify the foot orientation with respect to the cylinder in order to adjust the ZMP position.

On the other hand, the problem of finding a cyclic gait for our system is similar to that of finding a limit cycle gait for passive and semi-passive walkers. The following subsections review some of the related work in this area.

A. Walking Cycle of Passive Walking Robots

Limit walking cycle is a fundamental topic in the research of passive biped robots. McGeer [13] first demonstrated that a passive biped robot can walk down a slope in a steady periodic gait without any active control. The only energy supply to the robot is the potential energy, which compensate the loss of energy when the swing leg hits the ground. After McGeer's pioneering work, many researchers investigated passive biped walking. Goswami *et al.* [14] and Garcia *et al.* [15] verified the existence and the stability of limit walking cycles. Osuka and Kirihara [16] first demonstrated this symmetric motion on a real passive robot. Collins et al. [17] built the first three-dimensional passive biped robot with knees. Ikemata *et al.* [18], [19] studied several factors that may affect the stability of a limit walking cycle, such as the support exchange, the stabilization of a fixed point, and the motion of the swing leg. Freidovich *et al.* [20] proposed a faster way to seek both stable and unstable limit cycles than traditional numerical routines.

B. Walking Cycle of Powered Passive Walkers

Without any actuation or energy input, a passive walking robot can only walk on a declining slope. However, with the help of one or more actuators to compensate the energy loss at heel strike, powered passive walkers are able to walk on flat, level, or uphill ground and have higher capability to handle disturbances. One energy-efficient way to add actuation is the use of actuated ankles [21], [22], [23], [24], [25]. Using the ankle push-off not only decreases the energy use [21], [22] but also increases limit cycle walkers' ability to reject disturbances [23]. The use of ankle actuation also allows a robot to achieve different walking speed in limit cycle walking [24]. It has also been shown with simulation that pushing off before the swing leg hits the ground is energetically more efficient than pushing off after the heel strike [25]. Actuation can also be added at the hip joint [26]. Harada *et al.* [27] applied the limit cycle based walking generation to a model of present humanoid robots with more active joints and flat feet.

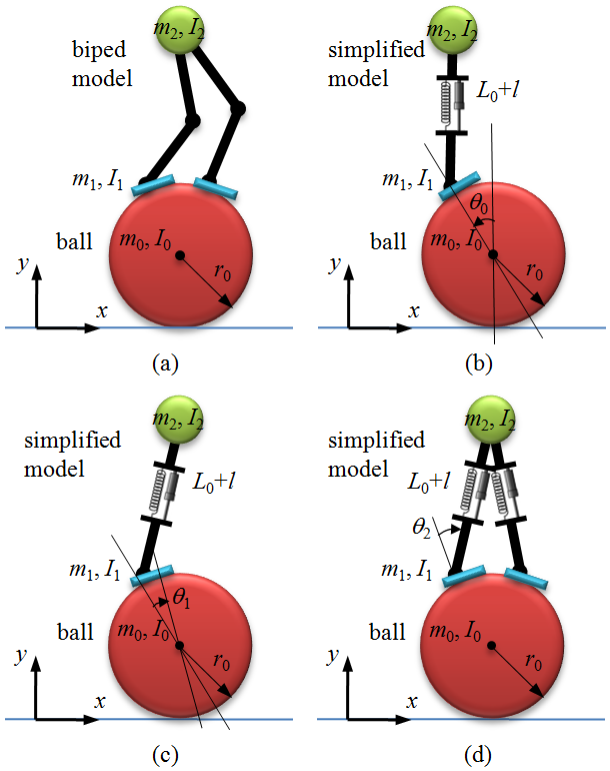

Fig. 2. Simplified dynamics model of a biped robot on a cylinder in the sagittal plane. (a) Biped model. (b) θ_0 is the rolling angle of the cylinder, which also indicates the relative position of the ankle joint to the top of the cylinder if the ankle joint is initially above the top. (c) θ_1 is the rolling angle of the foot relative to the cylinder. (d) θ_2 is the angle of the ankle joint, indicating the center of mass (CoM) position relative to the ankle.

III. Dynamics and Collision Models for the Walking Cycle Computation

In this section, we introduce the simplified model and the collision model.

A. Simplified Dynamics Model

Fig. 2 depicts our new simplified dynamics model of a biped robot on a cylinder. Let r_0, m_0, and I_0 respectively denote the radius, the mass, and the inertia of the cylinder, m_1 and I_1 the mass and the inertia of a foot, m_2 and I_2 the mass and inertia of the inverted pendulum, and $L = L_0+l$ the distance between the ankle joint and the lump mass, where L_0 is the distance while the robot is in the rest position and

l is the change of the distance. Here we assume that the CoM of each foot is at the ankle. For each leg, three angular variables θ_0, θ_1 and θ_2 as well as a linear variable l describe its configuration as indicated in Fig. 2, where θ_0 represents the rolling angle of the cylinder [Fig. 2(b)], θ_1 denotes the rolling angle of the foot relative to the cylinder [Fig. 2(c)], and θ_2 is the angle of the ankle joint [Fig. 2(d)]. Assume that there is no slip between the foot and the cylinder. The positive direction of angles is taken to be clockwise.

During the single support, the swing leg dynamics is ignored and the linearized equation of motion of the model can be written as

$$\boldsymbol{M}\ddot{\boldsymbol{\theta}} + \boldsymbol{G}\boldsymbol{\theta} = \boldsymbol{\tau} \tag{1}$$

where $\boldsymbol{\theta} = [\theta_0 \quad \theta_1 \quad \theta_2 \quad l]^T$, $\boldsymbol{\tau} = [0 \quad 0 \quad \tau_2 \quad f]^T$, τ_2 is the ankle torque, f is the spring-damper force and

$$\boldsymbol{M} = \begin{bmatrix} M_1 + I & M_2 + I_1 & M_2 & 0 \\ M_2 + I_1 & M_3 + I_1 & M_3 & 0 \\ M_2 & M_3 & M_3 & 0 \\ 0 & 0 & 0 & m_2 \end{bmatrix}$$

$$\boldsymbol{G} = -\begin{bmatrix} G_1 + m_2 g L_0 & m_2 g L_0 & m_2 g L_0 & 0 \\ m_2 g L_0 & m_2 g L_0 - G_1 & m_2 g L_0 & 0 \\ m_2 g L_0 & m_2 g L_0 & m_2 g L_0 & 0 \\ 0 & 0 & 0 & 0 \end{bmatrix}$$

$$M_1 = m_0 r_0^2 + 4 m_1 r_0^2 + m_2 L_1^2, \quad M_2 = m_2 L_0 L_1 + I_2$$
$$M_3 = m_2 l_0^2 + I_2, \quad L_1 = 2r_0 + L_0$$
$$I = I_0 + I_1 + I_2, \quad G_1 = (m_1 + m_2) g r_0.$$

We rewrite (1) as a state-space differential equation

$$\dot{\boldsymbol{x}} = \boldsymbol{A}\boldsymbol{x} + \boldsymbol{B}\boldsymbol{u} \tag{2}$$

where $\boldsymbol{x} = [\boldsymbol{\theta}^T \quad \dot{\boldsymbol{\theta}}^T]^T$ is the state, $\boldsymbol{u} = [\tau_2 \quad f]^T$ is the input, and the matrices $\boldsymbol{A}$ and $\boldsymbol{B}$ are given by

$$\boldsymbol{A} = \begin{bmatrix} \boldsymbol{0}_{4\times4} & \boldsymbol{I}_{4\times4} \\ -\boldsymbol{M}^{-1}\boldsymbol{G} & \boldsymbol{0}_{4\times4} \end{bmatrix}, \quad \boldsymbol{B} = \begin{bmatrix} \boldsymbol{0}_{4\times2} \\ \boldsymbol{M}^{-1}\begin{bmatrix} 0 & 0 \\ 0 & 0 \\ 1 & 0 \\ 0 & 1 \end{bmatrix} \end{bmatrix}.$$

Following [28], [12], we design a state-feedback balance controller as

$$\boldsymbol{u} = \boldsymbol{K}(\boldsymbol{x}^* - \boldsymbol{x}) \tag{3}$$

where $\boldsymbol{K} \in \mathbb{R}^{2\times8}$ is a feedback gain and $\boldsymbol{x}^*$ is an equilibrium state such that $\boldsymbol{A}\boldsymbol{x}^* = \boldsymbol{0}$. The first row of $\boldsymbol{K}$ consists of feedback gains for generating τ_2, while the second row contains the spring and damper coefficients for generating f. Since $\boldsymbol{A}$ here has full rank, $\boldsymbol{x}^* = \boldsymbol{0}$ is the only equilibrium state. Then substituting (3) into (2) yields

$$\dot{\boldsymbol{x}} = (\boldsymbol{A} - \boldsymbol{B}\boldsymbol{K})\boldsymbol{x}. \tag{4}$$

Therefore, we can easily solve (4) for $\boldsymbol{x}$ as

$$\boldsymbol{x} = e^{(\boldsymbol{A}-\boldsymbol{B}\boldsymbol{K})t}\boldsymbol{x}_0 \tag{5}$$

where $\boldsymbol{x}_0$ is the initial state. The feedback gain $\boldsymbol{K}$ is chosen so that it ensures that all the eigenvalues of $\boldsymbol{A} - \boldsymbol{B}\boldsymbol{K}$ have negative real parts and the system asymptotically converges to the equilibrium state.

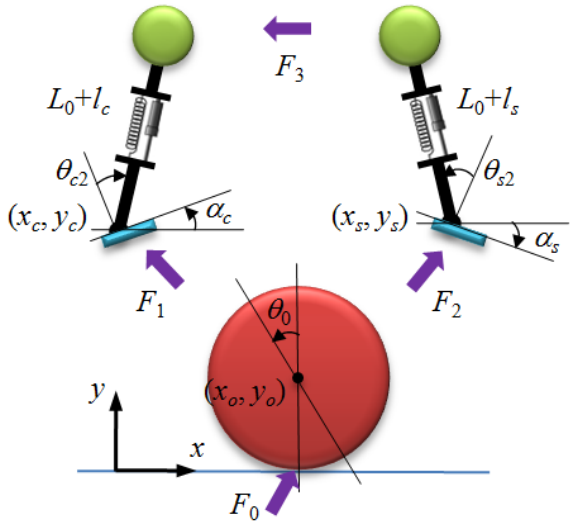

Fig. 3. Collision model. The motion of the cylinder is described using variables x_o, y_o, θ_0, while that of each leg is described using variables $x, y, \alpha, \theta_2, l$. The subscripts c and s represent the colliding (swing) leg and the supporting leg, respectively.

A real biped robot is usually equipped with several sensors, which may help us measure the actual values of all state variables. Assume that the cylinder's cross section is a perfect circle with known radius. A force-torque sensor at the ankle can give θ_1. With joint angle sensors, we can compute θ_2 and l. Then we can derive θ_0 from θ_2 and the global orientation of the feet, which can be acquired by using an inertial measurement unit at the robot's root. Finally, we can estimate the velocities with an observer or a Kalman filter.

B. Collision Model

A collision discontinuously changes the state of the whole system when the swing leg touches the cylinder. To model this effect, we describe the motions of the cylinder and two legs separately using the variables summarized in Fig. 3. The configuration of the cylinder is represented by (x_o, y_o) and θ_0, which indicate the position and orientation of the cylinder, respectively. The configuration of a leg is determined by another five parameters; that is, (x, y) to represent the position of the ankle joint, α the angle of the foot with respect to the horizontal plane, and θ_2 and l have the same meaning as in the simplified dynamics model. Therefore, we describe the configurations of the cylinder, the swing leg, and the supporting leg respectively by the following vectors:

$$\boldsymbol{q}_o = [x_o \quad y_o \quad \theta_0]^T \tag{6}$$
$$\boldsymbol{q}_c = [x_c \quad y_c \quad \alpha_c \quad \theta_{c2} \quad l_c]^T \tag{7}$$
$$\boldsymbol{q}_s = [x_s \quad y_s \quad \alpha_s \quad \theta_{s2} \quad l_s]^T. \tag{8}$$

The subscripts "o", "c", and "s" represent the cylinder, the swing (colliding) leg, and the supporting leg, respectively.

The position of the contact between the cylinder and the floor can be written in terms of $\boldsymbol{q}_o$ as

$$\boldsymbol{p}_F = \begin{bmatrix} x_o - r_0\theta_0 \\ y_o - r_0 \end{bmatrix}. \tag{9}$$

Then the Jacobian matrix of $\boldsymbol{p}_F$ with respect to $\boldsymbol{q}_o$ is

$$\boldsymbol{J}_{FO} = \frac{\partial \boldsymbol{p}_F}{\partial \boldsymbol{q}_o} = \begin{bmatrix} 1 & 0 & -r_0 \\ 0 & 1 & 0 \end{bmatrix}. \tag{10}$$

The position of the contact between the cylinder and the swing leg on the cylinder can be expressed as

$$\boldsymbol{p}_{CO} = \begin{bmatrix} x_o + r_0\theta_0 \cos\alpha_c \\ y_o - r_0\theta_0 \sin\alpha_c \end{bmatrix}. \tag{11}$$

Then the Jacobian matrix of $\boldsymbol{p}_{CO}$ with respect to $\boldsymbol{q}_o$ is

$$\boldsymbol{J}_{CO} = \frac{\partial \boldsymbol{p}_{CO}}{\partial \boldsymbol{q}_o} = \begin{bmatrix} 1 & 0 & r_0 \cos\alpha_c \\ 0 & 1 & -r_0 \sin\alpha_c \end{bmatrix}. \tag{12}$$

The position of the contact between the swing leg and the cylinder on the leg can be expressed in terms of $\boldsymbol{q}_c$ as

$$\boldsymbol{p}_{OC} = \begin{bmatrix} x_c - \lambda \cos\alpha_c \\ y_c + \lambda \sin\alpha_c \end{bmatrix} \tag{13}$$

where $\lambda = (x_c - x_o)\cos\alpha_c - (y_c - y_o)\sin\alpha_c$ is treated as a constant. Then the Jacobian matrix of $\boldsymbol{p}_{OC}$ with respect to $\boldsymbol{q}_c$ can be calculated by

$$\boldsymbol{J}_{OC} = \frac{\partial \boldsymbol{p}_{OC}}{\partial \boldsymbol{q}_c} = \begin{bmatrix} 1 & 0 & \lambda \sin\alpha_c & 0 & 0 \\ 0 & 1 & \lambda \cos\alpha_c & 0 & 0 \end{bmatrix}. \tag{14}$$

The CoM position can be written in terms of $\boldsymbol{q}_c$ as

$$\boldsymbol{p}_{MC} = \begin{bmatrix} x_c + Ls_c \\ y_c + Lc_c \end{bmatrix} \tag{15}$$

where $s_c = \sin(\alpha_c + \theta_{c2})$ and $c_c = \cos(\alpha_c + \theta_{c2})$. The Jacobian matrix of $\boldsymbol{p}_{MC}$ with respect to $\boldsymbol{q}_c$ is

$$\boldsymbol{J}_{MC} = \frac{\partial \boldsymbol{p}_{MC}}{\partial \boldsymbol{q}_c} = \begin{bmatrix} 1 & 0 & Lc_c & Lc_c & s_c \\ 0 & 1 & -Ls_c & -Ls_c & c_c \end{bmatrix}. \tag{16}$$

Similarly, we can compute those Jacobian matrices $\boldsymbol{J}_{SO}$, $\boldsymbol{J}_{OS}$, and $\boldsymbol{J}_{MS}$ for the supporting leg by simply substituting $\boldsymbol{q}_s$ for $\boldsymbol{q}_c$ in the above equations.

From now on, we denote by $\dot{\boldsymbol{q}}_o$, $\dot{\boldsymbol{q}}_c$, and $\dot{\boldsymbol{q}}_s$ respectively the velocities of the cylinder, the swing leg, and the supporting leg, and use superscripts $-$ and $+$ to distinguish quantities before and after collision. Let $\boldsymbol{F}_0$, $\boldsymbol{F}_1$, $\boldsymbol{F}_2$, and $\boldsymbol{F}_3$ denote the impulses at three contacts and the hip joint, as depicted in Fig. 3. From the conservation of momentum we have

$$\boldsymbol{M}_O(\dot{\boldsymbol{q}}_o^+ - \dot{\boldsymbol{q}}_o^-) = \boldsymbol{J}_{FO}^T\boldsymbol{F}_0 - \boldsymbol{J}_{CO}^T\boldsymbol{F}_1 - \boldsymbol{J}_{SO}^T\boldsymbol{F}_2 \tag{17a}$$

$$\boldsymbol{M}_C(\dot{\boldsymbol{q}}_c^+ - \dot{\boldsymbol{q}}_c^-) = \boldsymbol{J}_{OC}^T\boldsymbol{F}_1 + \boldsymbol{J}_{MC}^T\boldsymbol{F}_3 \tag{17b}$$

$$\boldsymbol{M}_S(\dot{\boldsymbol{q}}_s^+ - \dot{\boldsymbol{q}}_s^-) = \boldsymbol{J}_{OS}^T\boldsymbol{F}_2 - \boldsymbol{J}_{MS}^T\boldsymbol{F}_3 \tag{17c}$$

where

$$\boldsymbol{M}_O = \begin{bmatrix} m_0 & 0 & 0 \\ 0 & m_0 & 0 \\ 0 & 0 & I_0 \end{bmatrix}$$

$$\boldsymbol{M}_C = \begin{bmatrix} m_1 + m_2 & 0 & m_2Lc_c & m_2Ls_c & m_2s_c \\ 0 & m_1 + m_2 & -m_2Ls_c & -m_2Ls_c & m_2c_c \\ m_2Lc_c & -m_2Ls_c & M_3 + I_1 & M_3 & 0 \\ m_2Lc_c & -m_2Ls_c & M_3 & M_3 & 0 \\ m_2s_c & m_2c_c & 0 & 0 & m_2 \end{bmatrix}$$

and $\boldsymbol{M}_S$ has the same form as $\boldsymbol{M}_C$ by replacing s_c and c_c with $s_s = \sin(\alpha_s + \theta_{s2})$ and $c_s = \cos(\alpha_s + \theta_{s2})$, respectively.

The contact impulses $\boldsymbol{F}_0$, $\boldsymbol{F}_1$, $\boldsymbol{F}_2$ should also satisfy the friction constraint, which can be expressed as the following linear inequality constraints:

$$\boldsymbol{N}_0^T\boldsymbol{F}_0 \geq \boldsymbol{0}_{2\times 1}, \quad \boldsymbol{N}_1^T\boldsymbol{F}_1 \geq \boldsymbol{0}_{2\times 1}, \quad \boldsymbol{N}_2^T\boldsymbol{F}_2 \geq \boldsymbol{0}_{2\times 1} \tag{18}$$

where

$$\boldsymbol{N}_0^T = \begin{bmatrix} 1 & \mu \\ -1 & \mu \end{bmatrix}$$

$$\boldsymbol{N}_1^T = \begin{bmatrix} \mu\sin\alpha_c + \cos\alpha_c & \mu\cos\alpha_c - \sin\alpha_c \\ \mu\sin\alpha_c + \cos\alpha_c & -\mu\cos\alpha_c + \sin\alpha_c \end{bmatrix}$$

$$\boldsymbol{N}_2^T = \begin{bmatrix} \mu\sin\alpha_s + \cos\alpha_s & \mu\cos\alpha_s - \sin\alpha_s \\ \mu\sin\alpha_s + \cos\alpha_s & -\mu\cos\alpha_s + \sin\alpha_s \end{bmatrix}$$

and μ is the friction coefficient.

To ensure pure rolling of the cylinder on the floor before and after collision, we have the following equations

$$\boldsymbol{J}_{FO}\dot{\boldsymbol{q}}_o^- = \boldsymbol{0}_{2\times 1} \tag{19a}$$

$$\boldsymbol{J}_{FO}\dot{\boldsymbol{q}}_o^+ = \boldsymbol{0}_{2\times 1}. \tag{19b}$$

We also require no slip at the contact between the swing leg and the cylinder after collision, i.e.,

$$\boldsymbol{J}_{CO}\dot{\boldsymbol{q}}_o^+ - \boldsymbol{J}_{OC}\dot{\boldsymbol{q}}_c^+ = \boldsymbol{0}_{2\times 1}. \tag{20}$$

The supporting leg also maintains a nonslip contact with the cylinder before and after collision. Thus,

$$\boldsymbol{J}_{SO}\dot{\boldsymbol{q}}_o^- - \boldsymbol{J}_{OS}\dot{\boldsymbol{q}}_s^- = \boldsymbol{0}_{2\times 1} \tag{21a}$$

$$\boldsymbol{J}_{SO}\dot{\boldsymbol{q}}_o^+ - \boldsymbol{J}_{OS}\dot{\boldsymbol{q}}_s^+ = \boldsymbol{0}_{2\times 1}. \tag{21b}$$

Moreover, the linear velocities of the hip joint calculated from the swing and supporting legs must be the same, i.e.,

$$\boldsymbol{J}_{MS}\dot{\boldsymbol{q}}_s^- - \boldsymbol{J}_{MC}\dot{\boldsymbol{q}}_c^- = \boldsymbol{0}_{2\times 1} \tag{22a}$$

$$\boldsymbol{J}_{MS}\dot{\boldsymbol{q}}_s^+ - \boldsymbol{J}_{MC}\dot{\boldsymbol{q}}_c^+ = \boldsymbol{0}_{2\times 1}. \tag{22b}$$

IV. Computing a Cyclic Walking Gait

Let T denote a given step duration. We shall determine an initial state $\boldsymbol{x}_{s0} = \begin{bmatrix} \boldsymbol{\theta}_{s0}^T & \dot{\boldsymbol{\theta}}_{s0}^T \end{bmatrix}^T$ for the supporting leg such that after the time T, the swing leg collides with the cylinder and achieves the same initial state for the next step. We can reduce this problem into an optimization problem with respect to $\boldsymbol{x}_{s0}$ because the motion of the supporting leg depends only on its initial state, as indicated by (5).

A. Cost Function of the Optimization

The cost function consists of two parts, i.e., the difference between the initial and final CoM positions in a step and the difference between the initial states of two successive steps.

Given $\boldsymbol{x}_{s0}$, from (5) we can obtain the final state of the supporting leg after the time T, which is written as $\boldsymbol{x}_{sf} = \begin{bmatrix} \boldsymbol{\theta}_{sf}^T & \dot{\boldsymbol{\theta}}_{sf}^T \end{bmatrix}^T$. The position of the CoM relative to the center of the cylinder at a state $\boldsymbol{x}_s$ can be calculated by

$$\boldsymbol{p}_s = \begin{bmatrix} r_0(\sin\theta_{s01} - \theta_{s1}\cos\theta_{s01}) + L\sin\theta_{s02} \\ r_0(\cos\theta_{s01} + \theta_{s1}\sin\theta_{s01}) + L\cos\theta_{s02} \end{bmatrix} \tag{23}$$

where $\theta_{s01} = \theta_{s0} + \theta_{s1}$ and $\theta_{s02} = \theta_{s01} + \theta_{s2}$. Let $\boldsymbol{p}_{s0}$ and $\boldsymbol{p}_{sf}$ denote the CoM positions given by (23) at the initial

state $\boldsymbol{x}_{s0}$ and the final state $\boldsymbol{x}_{sf}$, respectively. We expect $\boldsymbol{p}_{sf} = \boldsymbol{p}_{s0}$ such that $\boldsymbol{\theta}_{c0} = [\theta_{c0} \quad \theta_{c1} \quad \theta_{c2} \quad l_c]^T$ of the swing leg before and after collision can equal the initial value $\boldsymbol{\theta}_{s0}$ of the supporting leg. The error between $\boldsymbol{p}_{s0}$ and $\boldsymbol{p}_{sf}$ is represented as

$$e_{\mathrm{CoM}} = \frac{1}{2}(\boldsymbol{p}_{sf} - \boldsymbol{p}_{s0})^T \boldsymbol{W}_P (\boldsymbol{p}_{sf} - \boldsymbol{p}_{s0}). \tag{24}$$

Assume that $\boldsymbol{\theta}_{c0}$ reaches the same value as $\boldsymbol{\theta}_{s0}$. Then we expect that $\dot{\boldsymbol{\theta}}_{c0}$ is also equal to $\dot{\boldsymbol{\theta}}_{s0}$. To determine $\dot{\boldsymbol{\theta}}_{c0}$, we need to compute the collision model presented in Section III-B. In computing the matrices $\boldsymbol{M}_C$, $\boldsymbol{N}_1$, $\boldsymbol{J}_{CO}$, $\boldsymbol{J}_{OC}$, $\boldsymbol{J}_{MC}$ in the collision model, we take $x_o = 0$, $y_o = 0$, $x_c = r_0 \sin(\theta_{s0} + \theta_{s1}) - r_0 \theta_{s1} \cos(\theta_{s0} + \theta_{s1})$, $y_c = r_0 \cos(\theta_{s0} + \theta_{s1}) + r_0 \theta_{s1} \sin(\theta_{s0} + \theta_{s1})$, $\alpha_c = \theta_{s0} + \theta_{s1}$, and $\theta_{c2} = \theta_{s2}$, where θ_{s0}, θ_{s1}, and θ_{s2} are the components of $\boldsymbol{\theta}_{s0}$. The computation of $\boldsymbol{M}_S$, $\boldsymbol{N}_2$, $\boldsymbol{J}_{SO}$, $\boldsymbol{J}_{OS}$, and $\boldsymbol{J}_{MS}$ is similar except that θ_{s0}, θ_{s1}, and θ_{s2} are the components of $\boldsymbol{\theta}_{sf}$.

In the collision model, the velocities $\dot{\boldsymbol{q}}_o^-$, $\dot{\boldsymbol{q}}_o^+$, $\dot{\boldsymbol{q}}_c^-$, $\dot{\boldsymbol{q}}_c^+$, $\dot{\boldsymbol{q}}_s^-$, $\dot{\boldsymbol{q}}_s^+$ and the impulses $\boldsymbol{F}_0$, $\boldsymbol{F}_1$, $\boldsymbol{F}_2$, $\boldsymbol{F}_3$ are the quantities to be determined. Here, $\dot{\boldsymbol{q}}_o^-$ and $\dot{\boldsymbol{q}}_s^-$ can be calculated from $\boldsymbol{x}_{sf}$ as

$$\dot{\boldsymbol{q}}_o^- = \begin{bmatrix} r_0\dot{\theta}_{s0} & 0 & \dot{\theta}_{s0} \end{bmatrix}^T \tag{25}$$

$$\dot{\boldsymbol{q}}_s^- = \begin{bmatrix} R_{11}\dot{\theta}_{s0} + R_{12}\dot{\theta}_{s1} & R_{21}\dot{\theta}_{s0} + R_{22}\dot{\theta}_{s1} & \dot{\theta}_{s01} & \dot{\theta}_{s2} & \dot{l}_s \end{bmatrix}^T \tag{26}$$

where $R_{11} = r_0(1 + \cos\theta_{s01} + \theta_{s1}\sin\theta_{s01})$, $R_{12} = r_0\theta_{s1}\sin\theta_{s01}$, $R_{21} = r_0(\theta_{s1}\cos\theta_{s01} - \sin\theta_{s01})$, $R_{22} = r_0\theta_{s1}\cos\theta_{s01}$, $\theta_{s01} = \theta_{s0} + \theta_{s1}$, $\dot{\theta}_{s01} = \dot{\theta}_{s0} + \dot{\theta}_{s1}$ and θ_{s0}, θ_{s1}, θ_{s2}, $\dot{\theta}_{s0}$, $\dot{\theta}_{s1}$, and $\dot{\theta}_{s2}$ are the components of $\boldsymbol{x}_{sf}$. It can be verified that $\dot{\boldsymbol{q}}_o^-$ and $\dot{\boldsymbol{q}}_s^-$ satisfy (19a) and (21a), respectively. The other contact constraints in (19)–(22) together with (17) can be rewritten in the matrix form

$$\boldsymbol{Q}\dot{\boldsymbol{q}} = \boldsymbol{b} \tag{27}$$

where $\dot{\boldsymbol{q}} = [\dot{\boldsymbol{q}}_o^+ \quad \dot{\boldsymbol{q}}_s^+ \quad \dot{\boldsymbol{q}}_c^+ \quad \dot{\boldsymbol{q}}_c^- \quad \boldsymbol{F}_0 \quad \boldsymbol{F}_1 \quad \boldsymbol{F}_2 \quad \boldsymbol{F}_3]^T \in \mathbb{R}^{26}$, $\boldsymbol{Q} \in \mathbb{R}^{23\times 26}$, $\boldsymbol{b} \in \mathbb{R}^{23}$, and

$$\boldsymbol{Q} = \begin{bmatrix} \boldsymbol{M}_O & \boldsymbol{0}_{3\times5} & \boldsymbol{0}_{3\times5} & \boldsymbol{0}_{3\times5} & -\boldsymbol{J}_{FO}^T & \boldsymbol{J}_{CO}^T & \boldsymbol{J}_{SO}^T & \boldsymbol{0}_{3\times2} \\ \boldsymbol{0}_{5\times3} & \boldsymbol{0}_{5\times5} & -\boldsymbol{M}_C & \boldsymbol{M}_C & \boldsymbol{0}_{5\times2} & \boldsymbol{J}_{OC}^T & \boldsymbol{0}_{5\times2} & \boldsymbol{J}_{MC}^T \\ \boldsymbol{0}_{5\times3} & \boldsymbol{M}_S & \boldsymbol{0}_{5\times5} & \boldsymbol{0}_{5\times5} & \boldsymbol{0}_{5\times2} & \boldsymbol{0}_{5\times2} & -\boldsymbol{J}_{OS}^T & \boldsymbol{J}_{MS}^T \\ \boldsymbol{J}_{FO} & \boldsymbol{0}_{2\times5} & \boldsymbol{0}_{2\times5} & \boldsymbol{0}_{2\times5} & \boldsymbol{0}_{2\times2} & \boldsymbol{0}_{2\times2} & \boldsymbol{0}_{2\times2} & \boldsymbol{0}_{2\times2} \\ \boldsymbol{J}_{CO} & \boldsymbol{0}_{2\times5} & -\boldsymbol{J}_{CO} & \boldsymbol{0}_{2\times5} & \boldsymbol{0}_{2\times2} & \boldsymbol{0}_{2\times2} & \boldsymbol{0}_{2\times2} & \boldsymbol{0}_{2\times2} \\ \boldsymbol{J}_{SO} & -\boldsymbol{J}_{SO} & \boldsymbol{0}_{2\times5} & \boldsymbol{0}_{2\times5} & \boldsymbol{0}_{2\times2} & \boldsymbol{0}_{2\times2} & \boldsymbol{0}_{2\times2} & \boldsymbol{0}_{2\times2} \\ \boldsymbol{0}_{2\times3} & \boldsymbol{0}_{2\times5} & \boldsymbol{0}_{2\times5} & \boldsymbol{J}_{MC} & \boldsymbol{0}_{2\times2} & \boldsymbol{0}_{2\times2} & \boldsymbol{0}_{2\times2} & \boldsymbol{0}_{2\times2} \\ \boldsymbol{0}_{2\times3} & \boldsymbol{J}_{MS} & -\boldsymbol{J}_{MC} & \boldsymbol{0}_{2\times5} & \boldsymbol{0}_{2\times2} & \boldsymbol{0}_{2\times2} & \boldsymbol{0}_{2\times2} & \boldsymbol{0}_{2\times2} \end{bmatrix}$$

$$\boldsymbol{b} = \begin{bmatrix} (\boldsymbol{M}_O\dot{\boldsymbol{q}}_o^-)^T & \boldsymbol{0}_{1\times5} & (\boldsymbol{M}_s\dot{\boldsymbol{q}}_s^-)^T & \boldsymbol{0}_{1\times2} & \boldsymbol{0}_{1\times2} & \boldsymbol{0}_{1\times2} & \boldsymbol{0}_{1\times2} & (\boldsymbol{J}_{MS}\dot{\boldsymbol{q}}_s^-)^T \end{bmatrix}^T.$$

Equation (27) is underdetermined. The impulses $\boldsymbol{F}_0$, $\boldsymbol{F}_1$, $\boldsymbol{F}_2$ must also satisfy (18). From $\dot{\boldsymbol{q}}_o^+$ and $\dot{\boldsymbol{q}}_c^+$ we can derive

$$\dot{\boldsymbol{\theta}}_{c0} = \begin{bmatrix} 0 & 0 & 1 & 0 & 0 & 0 & 0 & 0 \\ 0 & 0 & -1 & 0 & 0 & 1 & 0 & 0 \\ 0 & 0 & 0 & 0 & 0 & 0 & 1 & 0 \\ 0 & 0 & 0 & 0 & 0 & 0 & 0 & 1 \end{bmatrix} \begin{bmatrix} \dot{\boldsymbol{q}}_o^+ \\ \dot{\boldsymbol{q}}_c^+ \end{bmatrix} = \boldsymbol{P}\dot{\boldsymbol{q}}. \tag{28}$$

We shall minimize the difference between $\dot{\boldsymbol{\theta}}_{c0}$ and $\dot{\boldsymbol{\theta}}_{s0}$, i.e.,

$$\begin{aligned} e_{\mathrm{state}} = \ & \text{minimize} \ \ \frac{1}{2}\|\boldsymbol{P}\dot{\boldsymbol{q}} - \dot{\boldsymbol{\theta}}_{s0}\|^2 \\ & \text{subject to} \ \ (18) \text{ and } (27). \end{aligned} \tag{29}$$

The minimum objective value e_{state} of (29) gives the error between $\dot{\boldsymbol{\theta}}_{c0}$ and $\dot{\boldsymbol{\theta}}_{s0}$ after collision, and it also gives the error between $\boldsymbol{x}_{c0}$ and $\boldsymbol{x}_{s0}$, since $\boldsymbol{\theta}_{c0}$ is taken to be $\boldsymbol{\theta}_{s0}$.

Therefore, the cost function to be minimized is

$$E = e_{\mathrm{CoM}} + e_{\mathrm{state}}. \tag{30}$$

From the above arguments, E is a function of $\boldsymbol{x}_{s0}$.

B. Constraints of the Optimization

Now we discuss the constraints on $\boldsymbol{x}_{s0}$. First, we require the contact point between the supporting foot and the cylinder to be within the sole during the entire step. Let l_h and l_t denote the distance between the ankle joint and the heel and toe respectively. Then θ_1 should be limited within $[-l_h/r_0, l_t/r_0]$. From (5) we have $\theta_1 = \boldsymbol{a}_2^T\boldsymbol{x}_{s0}$, where $\boldsymbol{a}_2^T$ is the second row of $e^{(\boldsymbol{A}-\boldsymbol{B}\boldsymbol{K})t}$. Then we have

$$-l_h/r_0 \le \min_{t\in[0,T]} \boldsymbol{a}_2^T\boldsymbol{x}_{s0}, \quad \max_{t\in[0,T]} \boldsymbol{a}_2^T\boldsymbol{x}_{s0} \le l_t/r_0. \tag{31}$$

Besides, we require the cylinder to roll at a desired average rolling velocity $\dot{\theta}_0^d$. From (5) this requirement can be expressed as

$$(\boldsymbol{a}_1^T - \boldsymbol{e}_1^T)\boldsymbol{x}_{s0} = \dot{\theta}_0^d T \tag{32}$$

where $\boldsymbol{a}_1^T$ is the first row of $e^{(\boldsymbol{A}-\boldsymbol{B}\boldsymbol{K})T}$ and $\boldsymbol{e}_1^T = [1 \quad \boldsymbol{0}_{1\times7}]$. Equation (32) implies that the initial state $\boldsymbol{x}_{s0}$ for achieving a desired average velocity lies on a hyperplane with normal $\boldsymbol{a}_1 - \boldsymbol{e}_1$ in the state space.

Combining the cost function (30) and the constraints (31) and (32), we formulate the computation of the initial state $\boldsymbol{x}_{s0}$ for cyclic walking as the following optimization problem

$$\begin{aligned} & \text{minimize} \ \ E \\ & \text{subject to} \ \ (31) \text{ and } (32). \end{aligned} \tag{33}$$

We pursue $\boldsymbol{x}_{s0}$, for which the minimum value of E is zero.

V. Maintaining a Cyclic Walking Gait

Because of modeling errors and external disturbances, the state of the supporting leg at the end of a walking cycle may be different from the planned gait. Consequently, the swing leg may not reach the desired states for a new walking cycle before and after collision. In this section, we discuss how to recompute its state so that the robot recovers the planned cyclic gait.

A. Inverse Kinematics

The final CoM position $\boldsymbol{p}_{sf}$, which can be obtained by (23) with respect to the final state $\boldsymbol{x}_{sf}$ of a cycle, may slightly deviate from the initial value $\boldsymbol{p}_{s0}$. Then $\boldsymbol{\theta}_{c0}$ cannot be the same as $\boldsymbol{\theta}_{s0}$ when the swing leg touches the cylinder. Hence, we compute the inverse kinematics (IK) with respect to $\boldsymbol{p}_{sf}$ and determine $\boldsymbol{\theta}_{c0}$. Here we use the pseudoinverse method for the IK [29]. For higher numerical stability near singularities, one can use damped least squares methods [30].

Similar to (23), the CoM position $\boldsymbol{p}_c$ with respect to $\boldsymbol{\theta}_c$ can be written as

$$\boldsymbol{p}_c = \begin{bmatrix} r_0(\sin\theta_{c01} - \theta_{c1}\cos\theta_{c01}) + L\sin\theta_{c02} \\ r_0(\cos\theta_{c01} + \theta_{c1}\sin\theta_{c01}) + L\cos\theta_{c02} \end{bmatrix} \tag{34}$$

where $\theta_{c01} = \theta_{c0} + \theta_{c1}$ and $\theta_{c02} = \theta_{c01} + \theta_{c2}$. Starting with an initial value of $\boldsymbol{\theta}_{c0}$, which can be taken to be $\boldsymbol{\theta}_{s0}$, the pseudoinverse method performs the following iteration to compute $\boldsymbol{\theta}_{c0}$ such that $\boldsymbol{p}_{c0} = \boldsymbol{p}_{sf}$:

$$\boldsymbol{\theta}_{c0} = \boldsymbol{\theta}_{c0} + \boldsymbol{J}^{\dagger}(\boldsymbol{p}_{sf} - \boldsymbol{p}_{c0}) \tag{35}$$

where $\boldsymbol{J} = \partial \boldsymbol{p}_c / \partial \boldsymbol{\theta}_c \in \mathbb{R}^{2\times 4}$ is the Jacobian matrix of $\boldsymbol{p}_c$ with respect to $\boldsymbol{\theta}_c$ and $\boldsymbol{J}^{\dagger}$ is the pseudoinverse of $\boldsymbol{J}$,

$$\boldsymbol{J} = \begin{bmatrix} r_0(1+\cos\theta_{c01}) + J_1 & J_1 & L\cos\theta_{c02} & \sin\theta_{c02} \\ J_2 - r_0\sin\theta_{c01} & J_2 & -L\sin\theta_{c02} & \cos\theta_{c02} \end{bmatrix}$$

$$J_1 = r_0\theta_{c1}\sin\theta_{c01} + L\cos\theta_{c02}$$

$$J_2 = r_0\theta_{c1}\cos\theta_{c01} - L\sin\theta_{c02}.$$

The iteration stops when $\|\boldsymbol{J}^{\dagger}(\boldsymbol{p}_{sf} - \boldsymbol{p}_{c0})\|$ is small enough.

B. Initial State for the Next Step

From the IK computation, we have obtained $\boldsymbol{\theta}_{c0}$, which specifies the position of the swing leg touching the cylinder. Now we determine $\dot{\boldsymbol{\theta}}_{c0}$ after collision to obtain the whole initial state $\boldsymbol{x}_{c0}$ for the robot to walk another step.

Here the collision model (27) still works. We also expect to achieve the desired average rolling velocity $\dot{\theta}_0^d$. Thus $\boldsymbol{x}_{c0}$ should satisfy (32), which can be rewritten as a linear equality constraint on $\dot{\boldsymbol{\theta}}_{c0}$:

$$\boldsymbol{a}_{12}^T\dot{\boldsymbol{\theta}}_{c0} = \dot{\theta}_0^d T - \left(\boldsymbol{a}_{11}^T - [1 \quad \boldsymbol{0}_{1\times 3}]\right)\boldsymbol{\theta}_{c0} \tag{36}$$

where $\boldsymbol{a}_{11}$ and $\boldsymbol{a}_{12}$ contain the first and last four components of $\boldsymbol{a}_1$, respectively. Combining (27), (28), and (36), we obtain

$$\begin{bmatrix} \boldsymbol{Q} \\ \boldsymbol{a}_{12}^T\boldsymbol{P} \end{bmatrix}\dot{\boldsymbol{q}} = \begin{bmatrix} \boldsymbol{b} \\ \dot{\theta}_0^d T - \left(\boldsymbol{a}_{11}^T - [1 \quad \boldsymbol{0}_{1\times 3}]\right)\boldsymbol{\theta}_{c0} \end{bmatrix}. \tag{37}$$

Once solving (37) for $\dot{\boldsymbol{q}}$, we can calculate $\dot{\boldsymbol{\theta}}_{c0}$ by (28). Nevertheless, (37) is an underdetermined system, which has an infinite number of solutions. In order to maintain a planned cyclic gait, we pursue the solution to (37) that minimizes the cost function defined as follow.

First, we wish to minimize the error in the CoM position at the end of each step. From (5) and (28), the final state of a step after collision can be written as

$$\boldsymbol{x}_{cf} = e^{(\boldsymbol{A}-\boldsymbol{B}\boldsymbol{K})T}\begin{bmatrix} \boldsymbol{\theta}_{c0} \\ \boldsymbol{P}\dot{\boldsymbol{q}} \end{bmatrix}. \tag{38}$$

Then we can compute the CoM position $\boldsymbol{p}_{cf}$ at the end of the step after collision as (23). Since $\boldsymbol{\theta}_{c0}$ has been determined by the IK computation, from (38) we see that $\boldsymbol{x}_{cf}$ is a function of $\dot{\boldsymbol{q}}$ and so is $\boldsymbol{p}_{cf}$. Let $\boldsymbol{x}_0^* = [\boldsymbol{\theta}^* \quad \dot{\boldsymbol{\theta}}^*]^T$ be an optimal initial state obtained by solving the optimization problem (33) and $\boldsymbol{p}^*$ the CoM position calculated by (23) with respect to $\boldsymbol{x}_0^*$. Thus the error in the CoM position is represented as

$$e_{\text{CoM}} = \frac{1}{2}(\boldsymbol{p}_{cf} - \boldsymbol{p})^T\boldsymbol{W}_p(\boldsymbol{p}_{cf} - \boldsymbol{p}) \tag{39}$$

where $\boldsymbol{p} = (1-k_p)\boldsymbol{p}_{sf} + k_p\boldsymbol{p}^*$ and $k_p \in [0,1]$.

We also intend to minimize the error in the initial state of each step, which is represented as

$$e_{\text{state}} = \frac{1}{2}(\dot{\boldsymbol{\theta}}_{c0} - \dot{\boldsymbol{\theta}})^T\boldsymbol{W}_s(\dot{\boldsymbol{\theta}}_{c0} - \dot{\boldsymbol{\theta}}) \tag{40}$$

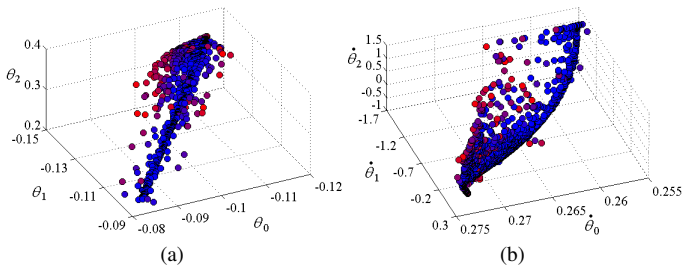

Fig. 4. Distribution of optimal initial states in the state space. Blue and red dots represent the optimal initial sates with smaller and larger values of the cost function defined by (30).

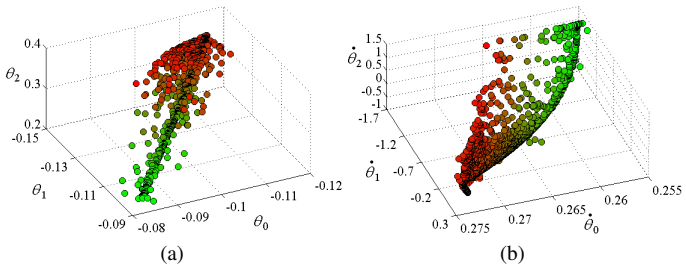

Fig. 5. Distribution of optimal initial states with smaller (marked in green) and larger (marked in red) energy consumption for one step.

where $\dot{\boldsymbol{\theta}} = (1-k_s)\dot{\boldsymbol{\theta}}_{s0} + k_s\dot{\boldsymbol{\theta}}^*$ and $k_s \in [0,1]$.

Therefore, the cost function is defined as $e_{\text{CoM}} + e_{\text{state}}$ and the solution for $\dot{\boldsymbol{q}}$ is reduced to the optimization problem

$$\begin{aligned} &\text{minimize} \quad e_{\text{CoM}} + e_{\text{state}} \\ &\text{subject to} \quad (37) \text{ and } (18). \end{aligned} \tag{41}$$

Using larger values for k_p and k_s, the resulting gait may be closer to the cyclic gait obtained from the optimization (33).

VI. Simulation Results

A. Setup for Optimization

The parameters of the simplified dynamics model are $m_0 = 157$ kg, $I_0 = 20$ kg$\cdot$m^2, $m_1 = 4$ kg, $I_1 = 0.05$ kg$\cdot$m^2, $m_2 = 61$ kg, $I_2 = 12$ kg$\cdot$m^2, $r_0 = 0.5$ m, and $L_0 = 0.8$ m. We set the step time $T = 0.5$ s and the desired average velocity $\dot{\theta}_0^d = 0.2$ rad/s. The upper and lower bounds on $\boldsymbol{x}_0$ are $\boldsymbol{x}_0^{\text{lb}} = [-\pi/4 \quad -0.15 \quad -\pi/2 \quad -\pi/2 \quad -\pi/2 \quad -\pi/2]^T$ and $\boldsymbol{x}_0^{\text{ub}} = [0 \;\; 0.15 \;\; \pi/2 \;\; \pi/2 \;\; \pi/2 \;\; \pi/2]^T$. We use the function **fmincon** provided by the Matlab Optimization Toolbox to solve (33).

B. Optimal Cyclic Gait

Fig. 4 shows the optimal initial states with slightly different minimized cost function values obtained by solving (33) with random initial values for the function **fmincon** between $\boldsymbol{x}_0^{\text{lb}}$ and $\boldsymbol{x}_0^{\text{ub}}$. Most of the optimal initial states have cost function values below 10^{-8}. In Fig. 5, the optimal initial states are colored according to the energy consumed in the step, which is estimated by the squared sum of ankle torques at every time step. It is clear that the gait with smaller initial $|\theta_0+\theta_1|$ has lower energy consumption, probably because the

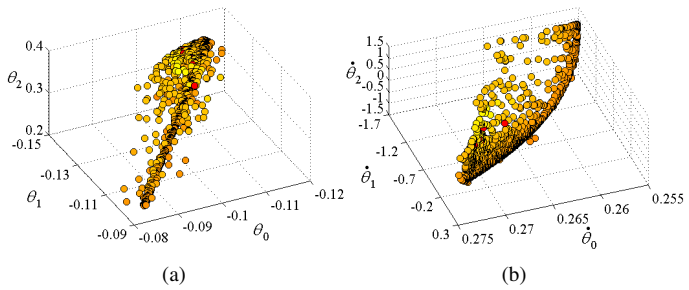

Fig. 6. Optimal initial states colored according to the change in the cost function while shifting optimal initial states in the normal direction. The yellow (red) color means that the change is relatively smaller (bigger).

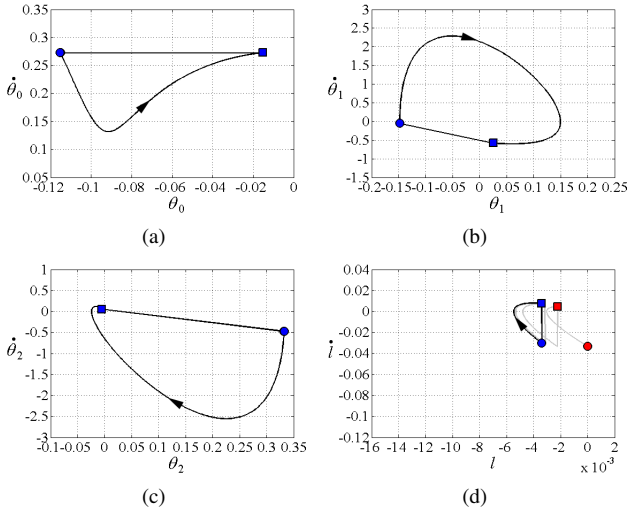

Fig. 7. One hundred walking cycles starting with an optimal initial state. Each curve from a dot to a square represents a step. The red color denotes the first step starting with the optimal initial state, while the blue color denotes the last step.

robot stands closer to the top of the cylinder and possesses larger potential energy. Equation (32) shows that the initial state lies on a hyperplane with normal $\boldsymbol{a}_1 - \boldsymbol{e}_1$. We slightly change each optimal initial state along the normal by the same amount and then plot optimal initial states in Fig. 6 colored according to the change of the cost function, which implies the robustness of a planned cyclic gait. It can be seen that the changes for most optimal initial states are similar.

Fig. 7 depicts 100 step cycles starting with an arbitrary optimal initial state. Due to the numerical error in the optimization, the spring-damper motion slightly deviates from the planned motion, as shown in Fig. 7(d). From Fig. 7(a) we see that the cylinder rolls 0.1 rad in one cycle, which implies that the average velocity is 0.2 rad/s and reaches the desired value, as the cycle period is 0.5 s.

C. Simulation Under Disturbance

We change the mass and inertia of the simulated model to $m_2 = 70$ kg and $I_2 = 15$ kg $\cdot$ m^2 to emulate the modeling error. We also add a Gaussian random error with zero mean and deviation of 0.2 N $\cdot$ m as the noise to the ankle torque at every time step. By the method proposed in Section V with

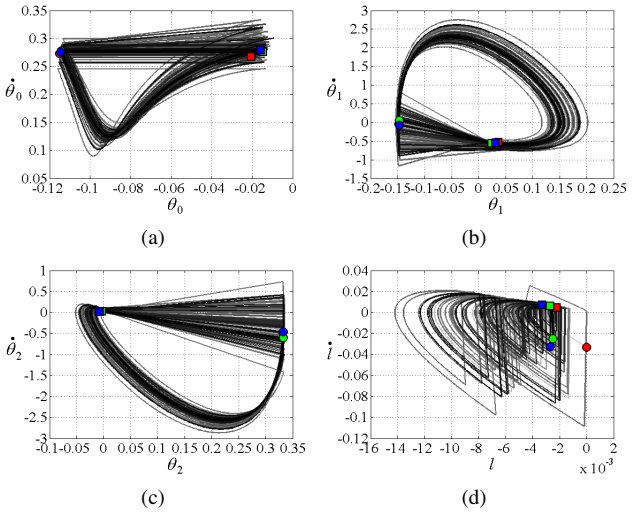

Fig. 8. Walking cycles under disturbances in the model and the ankle torque. The red color denotes the first step starting with the optimal initial state, while the green and blue colors denote the last two steps, which are slightly different due to the random disturbance.

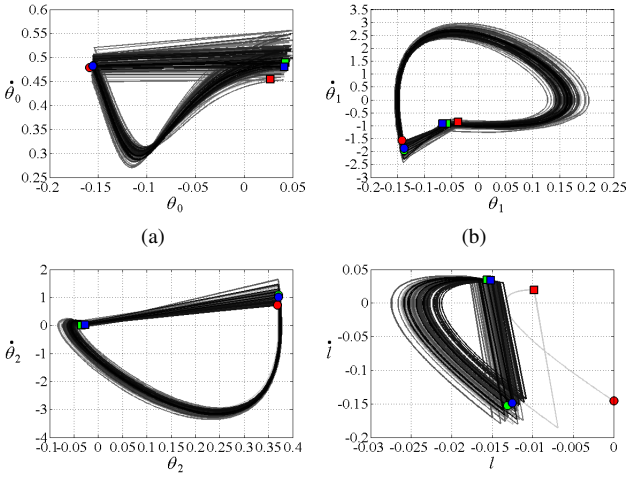

Fig. 9. Walking cycles with desired average velocity equal to 0.4 s^{-1}.

$k_p = 0.2$ and $k_s = 0.2$, the robot can still achieve stable cycles, as shown in Fig. 8. The cycles are slightly different from each other and those shown in Fig. 7 because of the disturbances in the model and the ankle torque. Nevertheless, the average velocity remains close to the desired value.

By our methods, we can achieve cyclic gaits with different average velocities even under larger disturbances, as shown in Fig. 9, where $\dot{\theta}_0^d = 0.4$ s^{-1}, $m_2 = 80$ kg and $I_2 = 20$ kg $\cdot$ m^2, and the deviation of the Gaussian random noise to the ankle torque is 0.5 N $\cdot$ m.

Fig. 10 displays the snapshots of one step of the two cyclic gaits, while the accompanying video exhibits 20 steps.

VII. Conclusion and Future Work

In this paper, we investigated the problem of generating and controlling cyclic bipedal walk on a rolling cylinder in the sagittal plane. We designed a balance control for a simplified linear model of the robot and derived a collision

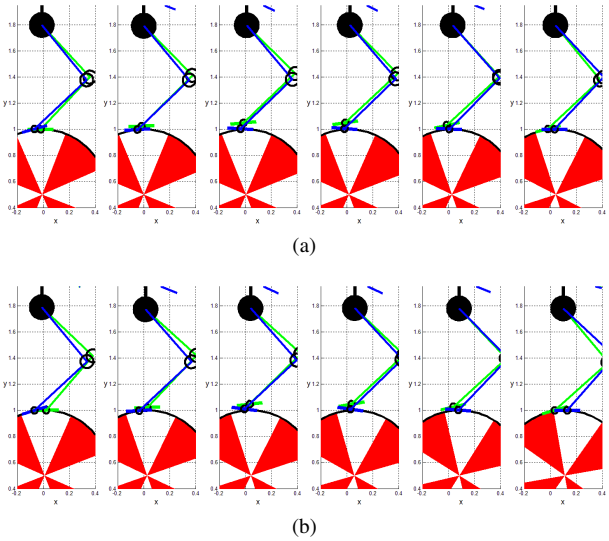

(a)

(b)

Fig. 10. Snapshots of one cyclic step with average velocity equal to (a) 0.2 rad/s and (b) 0.4 rad/s under different disturbances.

model for the supporting leg exchange. Then we established an optimization problem to compute the optimal initial state such that the robot can achieve a cyclic walking gait on the cylinder with a desired average rolling velocity. In consideration of modeling errors and external disturbance, we also proposed a method for determining an appropriate state of the swing leg before collision to maintain the robot in a stable cyclic gait. The effectiveness of our methods is demonstrated with simulations.

Our ultimate goal is to realize this motion on a real robot. To do this, there are many other issues that need to be considered. First, we shall explore how to bring the robot to a planned optimal initial state for a cyclic walk. Second, we would like to conduct the simulation with full-body dynamics rather than the simplified linear model. Third, we need to add an observer in our balance controller such that the state in the controller can keep close to the real state of the robot.

REFERENCES

[1] A. Takanishi, Y. Egusa, M. Tochizawa, T. Takeya, and I. Kato, "Realization of dynamic walking stabilized with trunk motion," in *CISM-IFToMM Symposium on Robot Design, Dynamics, and Control*, 1988, pp. 68–79.

[2] S. Kajita, T. Nagasaki, K. Kaneko, K. Yokoi, and K. Tanie, "A running controller of humanoid biped HRP-2LR," in *Proc. IEEE Int. Conf. Robot. Automat.*, Barcelona, Spain, 2005, pp. 616–622.

[3] J. Hodgins and M. Raibert, "Biped gymnastics," in *International Symposium of Robotics Research*, B. Bolles and B. Roth, Eds., 1987.

[4] S. Schaal and C. Atkeson, "Open loop stable control strategies for robot juggling," in *Proc. IEEE Int. Conf. Robot. Automat.*, 1993, pp. 913–918.

[5] Y. Kuroki, K. Kato, K. Nagasaka, A. Miyamoto, K. Ueno, and J. Yamaguchi, "Motion evaluating system for a small biped entertainment robot," in *Proc. IEEE Int. Conf. Robot. Automat.*, New Orieans, LA, 2004, pp. 3809–3814.

[6] J. Chestnutt, P. Michel, J. Kuffner, and T. Kanade, "Locomotion among dynamic obstacles for the Honda ASIMO," in *Proc. IEEE/RSJ Int. Conf. Intell. Robots Syst.*, San Diego, CA, 2007, pp. 2572–2573.

[7] S. O. Anderson and J. K. Hodgins, "Adaptive torque-based control of a humanoid robot on an unstable platform," in *Proc. IEEE-RAS Int. Conf. Humanoid Robots*, Nashville, TN, 2010, pp. 511–517.

[8] J. Pratt, J. Carff, S. Drakunov, and A. Goswami, "Capture point: a step toward humanoid push recovery," in *Proc. IEEE-RAS Int. Conf. Humanoid Robots*, Paris, France, 2006, pp. 200–207.

[9] S. Kudoh, T. Komura, and K. Ikeuchi, "Stepping motion for a human-like character to maintain balance against large peturbations," in *Proc. IEEE Int. Conf. Robot. Automat.*, Orlando, Florida, 2006, pp. 2661–2666.

[10] B. Stephens, "Humanoid push recovery," in *Proc. IEEE-RAS Int. Conf. Humanoid Robots*, Pittsburgh, PA, 2007, pp. 589–595.

[11] M. Stilman, J.-U. Schamburek, J. Kuffner, and T. Asfour, "Manipulation planning among movable obstacles," in *Proc. IEEE Int. Conf. Robot. Automat.*, Roma, Italy, 2007, pp. 3327–3332.

[12] Y. Zheng and K. Yamane, "Ball walker: A case study of humanoid robot locomotion in non-stationary environments," in *Proc. IEEE Int. Conf. Robot. Automat.*, Shanghai, China, 2011, pp. 2021–2028.

[13] T. McGeer, "Passive dynamic walking," *Int. J. Robot. Res.*, vol. 9, no. 2, pp. 62–82, 1990.

[14] A. Goswami, B. Thuilot, and B. Espiau, "A study of the passive gait of a compass-like biped robot: symmetry and chaos," *Int. J. Robot. Res.*, vol. 17, no. 12, pp. 1282–1301, 1998.

[15] M. Garcia, A. Chatterjee, A. Ruina, and M. Coleman, "The simplest walking model: stability, complexity, and scaling," *ASME J. of Biomech. Eng.*, vol. 120, pp. 281–288, 1998.

[16] K. Osuka and K. Kirihara, "Motion analysis and experiments of passive walking robot QUARTET II," in *Proc. IEEE Int. Conf. Robot. Automat.*, San Francisco, CA, 2000, pp. 3052–3056.

[17] S. H. Collins, M. Wisse, and A. Ruina, "A three-dimensional passive-dynamic walking robot with two legs and knees," *Int. J. Robot. Res.*, vol. 20, no. 7, pp. 607–615, 2001.

[18] Y. Ikemata, S. Akihito, and H. Fujimoto, "Analysis of limit cycle in passive walking," in *Proc. IEEE/RSJ Int. Conf. Intell. Robots Syst.*, Las Vegas, Nevada, 2003, pp. 601–606.

[19] Y. Ikemata, K. Yasuhara, A. Sano, and H. Fujimoto, "Generation and local stabilization of fixed point based on a stability mechanism of passive walking," in *Proc. IEEE Int. Conf. Robot. Automat.*, Pasadena, CA, 2008, pp. 1588–1593.

[20] L. B. Freidovich, U. Mettin, A. S. Shiriaev, and M. W. Spong, "A passive 2-DOF walker: hunting for gaits using virtual holonomic constraints," *IEEE Trans. Robot.*, vol. 25, no. 5, pp. 1202–1208, 2009.

[21] A. D. Kuo, "Energetics of actively powered locomotion using the simplest walking model," *ASME J. of Biomech. Eng.*, vol. 124, no. 2, pp. 113–120, 2002.

[22] S. H. Collins, A. Ruina, R. Tedrake, and M. Wisse, "Efficient bipedal robots based on passive-dynamic walkers," *Science*, vol. 307, no. 5712, pp. 1082–1085, 2005.

[23] D. G. E. Hobbelen and M. Wisse, "Ankle actuation for limit cycle walkers," *Int. J. Robot. Res.*, vol. 27, no. 6, pp. 709–735, 2008.

[24] ——, "Controlling the walking speed in limit cycle walking," *Int. J. Robot. Res.*, vol. 27, no. 9, pp. 989–1005, 2008.

[25] M. Franken, G. van Oort, and S. Stramigioli, "Analysis and simulation of fully actuated planar biped robots," in *Proc. IEEE/RSJ Int. Conf. Intell. Robots Syst.*, Nice, France, 2008, pp. 634–639.

[26] E. Dertien, "Dynamic walking with dribbel," *IEEE Robot. Automat. Mag.*, vol. 13, no. 3, pp. 118–121, 2006.

[27] Y. Harada, J. Takahashi, D. Nenchev, and D. Sato, "Limit cycle based walk of a powered 7DOF 3D biped with flat feet," in *Proc. IEEE/RSJ Int. Conf. Intell. Robots Syst.*, Taipei, Taiwan, 2010, pp. 3623–3628.

[28] K. Yamane and J. Hodgins, "Simultaneous tracking and balancing of humanoid robots for imitating human motion capture data," in *Proc. IEEE/RSJ Int. Conf. Intell. Robots Syst.*, St. Louis, 2009, pp. 2510–2517.

[29] D. E. Whitney, "Resolved motion rate control of manipulators and human prostheses," *IEEE Trans. Man. Mach. Syst.*, vol. 10, no. 2, pp. 47–53, 1969.

[30] Y. Nakamura and H. Hanafusa, "Inverse kinematics solutions with singulairty robustness for robot manipulator control," *ASME J. Dyn. Syst. Meas. Control*, vol. 108, no. 3, pp. 163–171, 1986.